Regular Article

Pattern formation in bubbles emerging periodically from a liquid free surface

H.N. Yoshikawa[1,a], C. Mathis[1,b], P. Maïssa[1,c], G. Rousseaux[1,d], and S. Douady[2,e]

[1] Laboratoire J.-A. Dieudonné, UMR 6621 CNRS/Université de Nice-Sophia Antipolis, Parc Valrose, 06108 Nice Cedex 02, France

[2] Matières et Systèmes Complexes, UMR 7057 CNRS/Université Paris-Diderot, 10 rue Alice Domon et Léonie Duquet, 75205 Paris Cedex 13, France

Abstract. Patterns formed by centimeter scale bubbles on the free surface of a viscous liquid are investigated in a cylindrical container. These bubbles emerge periodically at the surface and interact with each other in the central zone. Their radial emission, due to interaction and radial surface flow, leads to the formation of a variety of patterns. Different star-like and spiral patterns appear spontaneously by increasing the bubble emergence frequency. It is found that these patterns are due to a constant angular shift in the bubble emission direction. Measurements of this angular shift show a supercritical bifurcation accompanied by a transition from a pattern of two opposed straight arms to spiral patterns. By applying the tools and concepts from the study of leaf arrangement in botany (phyllotaxis), the recognized patterns and the mechanism of the pattern formation are discussed. Close similarities to the leaf arrangement are found in the behavior of the angular shift and the patterns. These findings suggest that the observed patterns are formed by a packing mechanism of successively appearing elements (bubbles), which is similar to that of the leaves at the earliest stage of phyllotaxis.

1 Introduction

The study of the arrangement of leaves on plant stems, *phyllotaxis*, has a long history. Theophrastus (370 B.C.-285 B.C.), in the Peripatetic school, left writing that shows ancient scholars' awareness of the regularity of leaf arrangement [1]. da Vinci (1452-1519) remarked that leaves on the stems of many plants are located at a constant angular shift around the stem and that seeds in a sunflower capitulum exhibit spiral patterns [2]. These features exhibited by plants are now described, respectively, in terms of the *divergence angle*, *i.e.*, the angular shift ψ between consecutive elements (leaves, seeds, etc.) and the *parastichies*, *i.e.*, the spirals determined by joining each element to its nearest neighbor to the right and to the left. The numbers of right and left parastichies characterize a pattern and are known to develop spatially. Schimper associated common divergence angles with the ratios of two successive terms of the Fibonacci sequence, which is defined by the recurrence relation $u_{n+1} = u_n + u_{n-1}$ $(n = 1, 2, \ldots)$ [3]. Auguste and

Louis Bravais considered the number of parastichies and related them to a unique divergence angle, $\psi_G = 2\pi(1-\tau)$, where τ is the golden mean $\tau = (\sqrt{5} - 1)/2$ and equal to $\lim(u_n/u_{n+1})$ [4,5]. Hofmeister attracted attention to the morphological process in the apex where the primordia of leaves are formed successively in the largest available space [6]. van Iterson computed a bifurcation diagram by considering packing and contact of the primordia. It enables one to deduce the divergence angle and the numbers of parastichies from the primordium size relative to the apex [7].

Very recently, a study on the crucial role of the plant hormone, auxin, in the patterning mechanism of phyllotaxis has been developed [8]. It was demonstrated that cellular carrier proteins are responsible for the transportation of auxin through plant tissues and that the heterogeneous nature of its accumulation is characterized by a minimum length of separation between the primordia. Physical modeling of the phyllotaxis has also started recently. Levitov calculated the energy of flux lattices in a layered superconductor [9]. He found that lattices at the ground state exhibit the same characteristics as the van Iterson diagram with pruned branches. Nisoli *et al.* performed an experiment with repulsive magnets on a cylinder and showed that their arrangement in a ground state is sim-
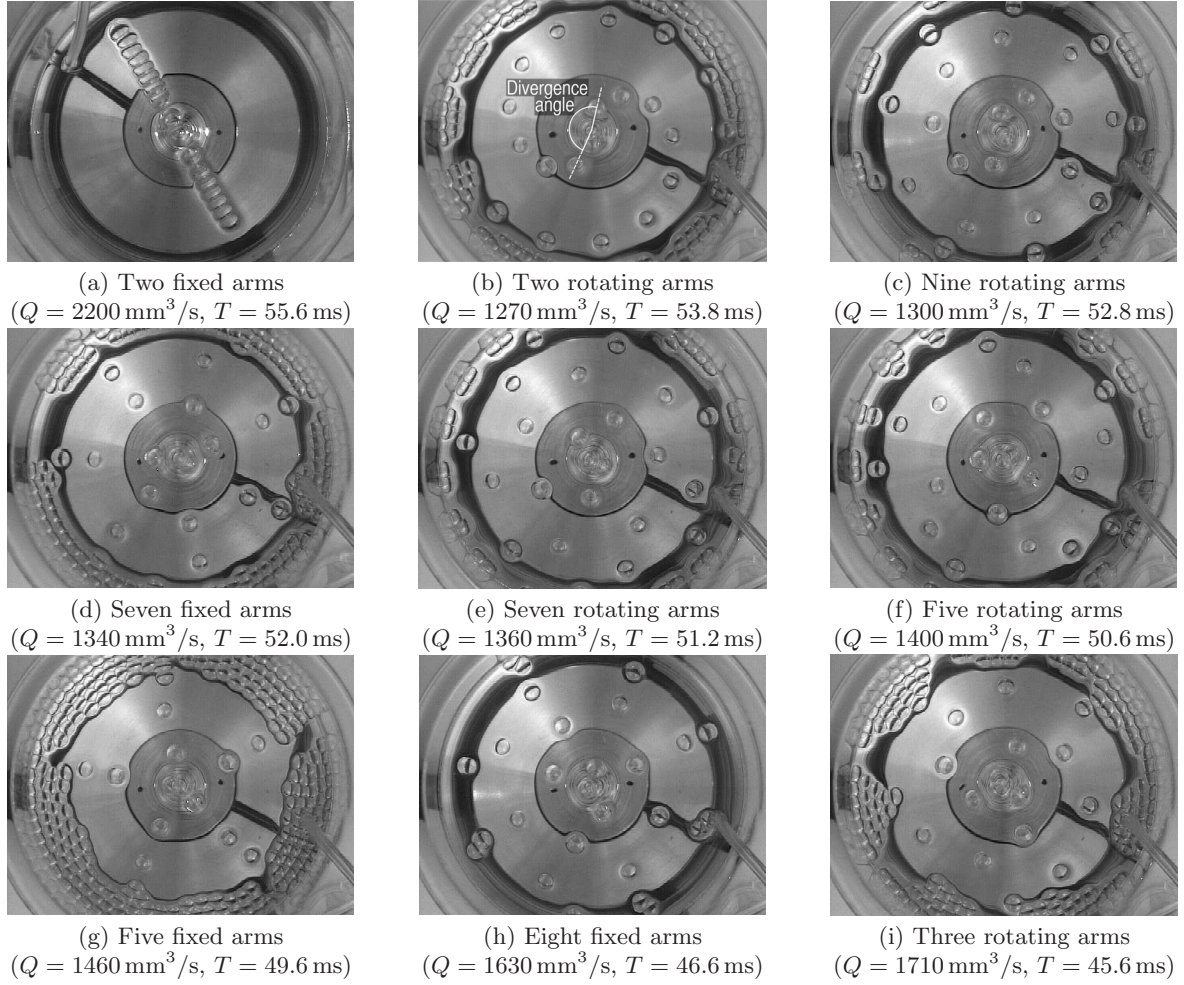
a e-mail: `harunori@unice.fr`
b e-mail: `Christian.Mathis@unice.fr`
c e-mail: `Philippe.Maissa@unice.fr`
d e-mail: `Germain.Rousseaux@unice.fr`
e e-mail: `stephane.douady@univ-paris-diderot.fr`

(a) Two fixed arms
($Q = 2200 \, \text{mm}^3/\text{s}$, $T = 55.6 \, \text{ms}$)

(b) Two rotating arms
($Q = 1270 \, \text{mm}^3/\text{s}$, $T = 53.8 \, \text{ms}$)

(c) Nine rotating arms
($Q = 1300 \, \text{mm}^3/\text{s}$, $T = 52.8 \, \text{ms}$)

(d) Seven fixed arms
($Q = 1340 \, \text{mm}^3/\text{s}$, $T = 52.0 \, \text{ms}$)

(e) Seven rotating arms
($Q = 1360 \, \text{mm}^3/\text{s}$, $T = 51.2 \, \text{ms}$)

(f) Five rotating arms
($Q = 1400 \, \text{mm}^3/\text{s}$, $T = 50.6 \, \text{ms}$)

(g) Five fixed arms
($Q = 1460 \, \text{mm}^3/\text{s}$, $T = 49.6 \, \text{ms}$)

(h) Eight fixed arms
($Q = 1630 \, \text{mm}^3/\text{s}$, $T = 46.6 \, \text{ms}$)

(i) Three rotating arms
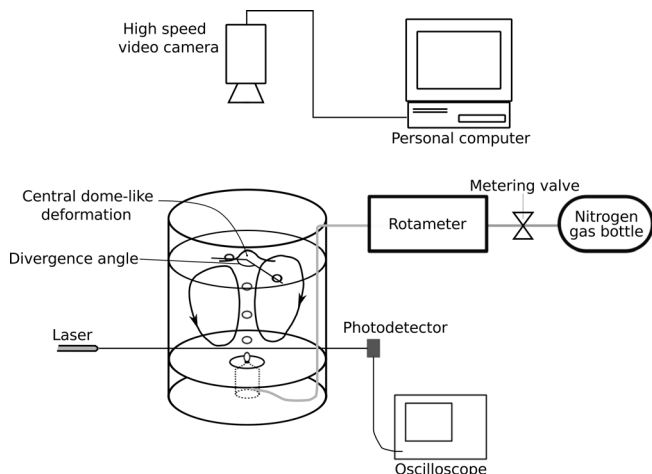($Q = 1710 \, \text{mm}^3/\text{s}$, $T = 45.6 \, \text{ms}$)

Fig. 1. Different patterns formed by bubbles emerging at the surface of silicone oil with different periods T ($\mu = 0.033 \, \text{Pa s}$, $d = 0.8 \, \text{mm}$, $H = 87 \, \text{mm}$ except the first picture, for which $\mu = 0.072 \, \text{Pa s}$, $d = 1.4 \, \text{mm}$, $H = 78 \, \text{mm}$). The patterns (b)-(i) are obtained by increasing the flow rate Q of the gas.

ilar to phyllotaxis [10]. Douady and Couder considered the phyllotaxis to be a self-organizing iterated process and implemented an original physical experiment [11–14]. Drops of water-based ferrofluid were released with a constant period and fell in silicone oil towards a circular bump placed at the center of a flat bottom. The system was subjected to a magnetic field gradient so that magnetized drops were repelled from each other and advected radially at the bottom. By the repulsion and advection, they simulated the packing effect in the apex and the growth of a plant, and succeeded in reproducing different spiral patterns similar to botanical ones. Numerical and theoretical computations showed how the van Iterson bifurcation diagram was pruned to explain the predominant occurrence of a divergence angle ψ_G in plants and the parastichy numbers composed of two successive terms of the Fibonacci sequence [11, 12, 15]. Other physical experiments showing spontaneous spiral generation can also be found in the literature, *e.g.*, the one performed by Habibi *et al.* [16]. They reported the hydrodynamic instability of a liquid filament

falling and coiling on a solid surface. Different patterns were formed by bubbles trapped in the coil and advected radially on the surface.

In the present paper, we report experiments performed with a novel physical system showing spontaneous *phyllotactic* pattern formation, *i.e.*, pattern formation caused by a packing-advection mechanism of successively appearing elements. The system is a simple hydrodynamic setup with circular symmetry and consists in a periodical emergence of centimeter-scale bubbles at a fixed point on a liquid surface. These bubbles ascend in line and interact with preceding and succeeding ones at the emergence point. They are then advected radially outward from the emergence point by a surface flow generated by the ascending bubbles themselves, forming regular patterns on the surface within a certain range of relevant parameters. In spite of the simplicity of the system, the variety of formed patterns is large: rotating and fixed multi-arms of bubbles are observed, as shown in fig. 1. A bifurcation from the pattern with two fixed arms (*e.g.*, fig. 1(a)) to other patterns
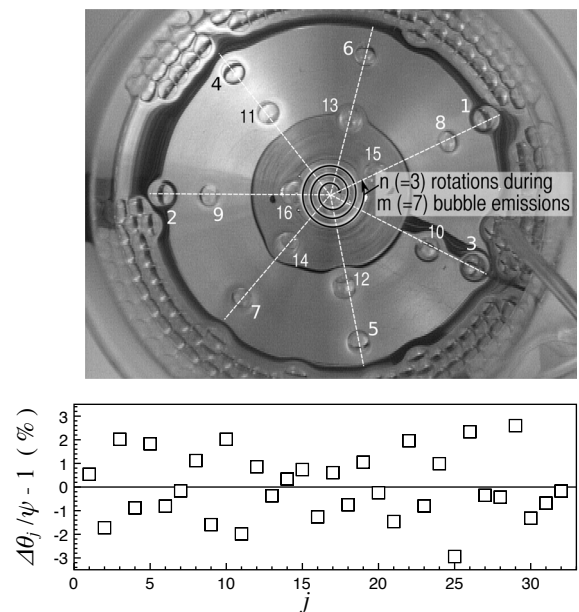
Fig. 2. Schematic illustration of the experimental setup.

Fig. 3. Bubble labeling and divergence angle measurement. Bubbles are labeled chronologically and the direction θ_j ($j = 1, 2, 3, \ldots$) of the radial motion of each bubble is measured. Determined divergence angles $\Delta\theta_j$ ($= \theta_{j+1} - \theta_j$) group well around their average value ψ.

with fixed and rotating arms (*e.g.*, fig. 1(b)-(i)) is found. After presenting our observations and measurements, we will discuss this bifurcation and show the relation of the present pattern formation to phyllotaxis.

2 Experimental setup and measurement techniques

The experimental setup consists of a vertical cylindrical container filled with a test liquid, a bubble formation device immersed in the liquid, a laser interception bubble detection system, a gas source and devices for optical observation (see fig. 2). The container is a glass beaker of inner diameter $R = 65$ mm and height 130 mm. Test liquids are silicone oils of different viscosities μ (density $\rho \approx 970$ kg/m^3 and surface tension $\gamma \approx 20$ mN/m for all the oils). The considered viscosities μ are 0.033, 0.048, 0.072 and 0.097 Pa s. The depth of the liquid, H, is typically 80 mm.

The bubble formation device is a chamber with a volume of approximately 8000 mm^3. This chamber has an inlet with a diameter of roughly 0.5 mm for gas supply and an opening closed by a screw top. Bubbles are formed at a circular orifice of diameter d at the center of the screw top. Different tops are prepared for different orifice diameters in the range $0.8 \leq d \leq 3.0$ mm. The bubble formation device is flush-mounted on a circular solid plate immersed at the bottom of the beaker. Nitrogen gas is supplied to the cavity from a compressed gas source and bubbles are formed at the orifice one by one with a constant interval T. The gas flow is controlled by a metering valve. Its flow rate Q is measured by a rotameter (BROOKS 1355). The range of Q is $140 \leq Q \leq 4200$ mm^3/s. The bubble formation period T is determined by the detection of bubble presence at the orifice. A low-power laser beam passes above the orifice at a distance of 2 mm. A photodetector aligned with the beam detects the presence or absence of

bubble formation by a low or high output signal, respectively. The signal is measured on an oscilloscope.

The volume of formed bubbles QT ranges between 30 and 250 mm^3. The corresponding volume-equivalent diameter $D_e = (6/\pi \cdot QT)^{1/3}$ lies between 3.9 mm and 7.8 mm. For a given orifice and a given liquid, the period T and the size D_e are controlled simultaneously by the flow rate Q.

A high-speed video camera (M30 JAI) is positioned above the container with the downward optical axis coincident with the container's central axis. The camera is used in combination with a digital image acquisition card (Imaging Tech. Inc.) to capture images of the liquid surface and bubbles at a typical rate of 120 images per second. The spatial resolution is typically 0.13 mm/pix. The images are stored on a personal computer for later analysis. Determination of the divergence angle ψ, *i.e.*, the angular difference of emission direction between two successive bubbles, is performed by measuring the azimuthal directions of the bubbles' radial motion in the top view images. Bubbles emerging at the surface are labeled chronologically as $j = 1, 2, 3, \ldots$ (see the picture in fig. 3). The direction θ_j of motion for the j-th emerging bubble is measured on images near the center of the surface (when the bubble is advected up to a distance of around $1.5D_e$ from the center). The divergences $\Delta\theta_j = \theta_{j+1} - \theta_j$ for different j are constant with fluctuations, as shown in the lower half of fig. 3. Their average value ψ is estimated from $\Delta\theta_j$ for at least 30 successive bubbles.

$t = 0\,\text{ms}$ $16.6\,\text{ms}$ $57.9\,\text{ms}$
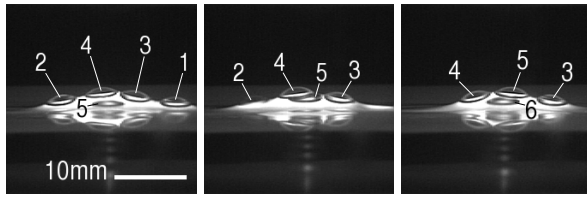
(a) Experiment yielding a pattern with two fixed arms
($Q = 280\,\text{mm}^3/\text{s}$, $T = 52\,\text{ms}$)

$t = 0\,\text{ms}$ $16.6\,\text{ms}$ $41.4\,\text{ms}$
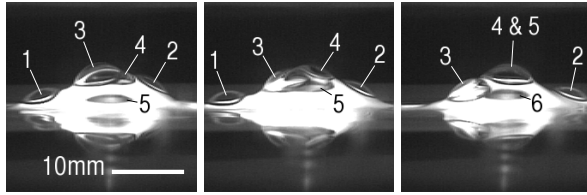
(b) Experiment yielding a pattern with two rotating arms
($Q = 1200\,\text{mm}^3/\text{s}$, $T = 36\,\text{ms}$)

Fig. 4. Successive side-view pictures of bubble behavior in the central deformed surface zone ($0.044\,\text{Pa s}$, $H = 174\,\text{mm}$, $d = 1.2\,\text{mm}$). Bubbles are numbered in order of appearance.

3 Results

3.1 Bubble motion

Bubbles form and grow up at the orifice of the bubble formation device from continuous gas supply. They detach at a certain size one by one from the orifice. The bubbles released into the liquid ascend vertically due to buoyancy. Although this ascending motion is first accelerated, the velocity of the bubbles is saturated by the viscous drag exerted by the liquid. This saturation occurs when the bubbles travel a distance of a few bubble diameters from the orifice, which is much smaller than the liquid height H. The bubbles impact the liquid surface with the terminal velocity and emerge at the surface.

At the point of the emergence, the surface deforms in the shape of a bell due to the upward liquid jet induced by the bubbles' rising motion. The deformation has an extent of a few bubble diameters. Inside this deformed surface zone, emerging bubbles interact with each other. An emerging bubble encounters and pushes the preceding ones near the top of the zone. In fig. 4, images captured by the high-speed video camera pointing horizontally at the central zone of the surface with a small downward tilt are shown for different flow rates. The luminous parts correspond to the deformed surface zone. At small flow rates that yield a divergence angle equal to π, as reported later in sect. 3.3, only two bubbles are in contact at the moment of radial bubble emission (see the central image in (a)). With higher flow rates, it is observed that three bubbles are in contact just before the emission as seen in the central image in (b). In the latter situation, the resulting divergence angle ψ is smaller than π. The deformed surface zone would be the analogue of the apex in plant systems where the primordia of leaves are packed and in

contact with each other. The pushed bubble is emitted radially from the center along the surface and can be advected further away by the radial surface flow of the liquid. This flow is generated by the bubble ascending motion, as illustrated in fig. 2, and provides an advection mechanism for phyllotactic pattern formation, similar to the radial gradient of a magnetic field in Douady and Couder's experiment. This simulates plant growth in botany.

3.2 Dimensionless groups

The considered hydrodynamic system can be characterized by eight parameters: the physical properties of the liquid, ρ, μ and γ, the geometrical parameters, R and H, the bubble formation characteristics, D_e and T, and the gravitational acceleration, g. The gas density and viscosity have been neglected, as the bubble pressure is atmospheric. Using dimensional analysis, one can construct five dimensionless groups from these parameters:

$$Bo = \frac{\rho g D_e^2}{\gamma}, \qquad Oh = \sqrt{\frac{\mu^2}{\rho \gamma D_e}}, \qquad \Omega = \frac{\rho D_e^2}{\mu T},$$

$$r_1 = \frac{H}{D_e} \quad \text{and} \quad r_2 = \frac{R}{D_e}. \tag{1}$$

The Bond number Bo is the square ratio of the bubble size D_e to the capillary length $(\gamma/\rho g)^{1/2}$. For the present experiments, the capillary length is $1.5\,\text{mm}$ and the number Bo ranges from 7.2 to 26. The Ohnesorge number Oh is the square root ratio of the viscous length scale $\mu^2/\rho\gamma$ to the bubble size. The value of this viscous length scale is $0.06\,\text{mm}$ for the least viscous oil ($0.033\,\text{Pa s}$) and $0.49\,\text{mm}$ for the most viscous one ($0.097\,\text{Pa s}$). The range of Oh is $0.11 \leq Oh \leq 0.27$. The dimensionless frequency Ω can also be regarded as a square ratio of the bubble size to the diffusive length scale $(\mu T/\rho)^{1/2}$. When pattern formation is observed at the surface, the latter length scale is typically $1.3\,\text{mm}$ in the least viscous oil and $2.5\,\text{mm}$ in the most viscous one. Ω lies between 7 and 19. The other two groups represent the confinement effects of the container. These were kept large ($10 \lesssim r_1 \lesssim 20$ and $8 \lesssim r_2 \lesssim 17$) for weak confinement. Their possible influence on pattern formation (*e.g.*, through global circulating flow in the container) is beyond the scope of the present paper and may be examined in a future publication. In the present work, the divergence angle ψ is given by a functional equation: $\psi = \mathcal{F}(Bo, Oh, \Omega)$.

3.3 Patterns

At small flow rates Q of gas injection, the advecting liquid flow is weak so that the capillary attraction between bubbles at the surface influence their behavior strongly. They are clustered or, with a relatively large Q, aligned on a radius. When the flow rate is larger than a certain value, bubbles are emitted horizontally from the emergence point one by one in alternate directions ($\psi = \pi$) and the pattern

exhibits two straight arms (see fig. 1(a)). This pattern has a central and two mirror symmetries and is analogous to the *alternate* mode in phyllotaxis. In each arm, bubbles are first in contact with each other due to the capillary force between them. The radial surface flow is not strong enough to overcome this attraction. Further increase of Q separates the bubbles in each arm by stronger advection flow, while the pattern remains the same ($\psi = \pi$).

When Q is increased above a certain threshold, the divergence angle ψ departs from π and the mirror symmetries are broken. Spiral patterns start to be seen. First, two rotating arms are formed as shown in fig. 1(b). To the observer's eye, these appear to rotate, while the motion of each bubble is purely radial. The orientation of the two arms is randomly chosen: it may change after a strong external perturbation such as a shock given to the container.

The divergence angle decreases with increasing Q and a variety of spiral patterns are formed at the surface. The series of pictures (b)-(i) in fig. 1 show patterns obtained by increasing the flow rate Q in a given liquid with a given orifice ($H = 78\,\mathrm{mm}$, $d = 1.4\,\mathrm{mm}$, $\mu = 0.072\,\mathrm{Pa\,s}$). At higher values of Q, the arms appear to rotate at a higher rate and more than two arms (nine, seven, five, eight, ... or even more) start to be visible, as seen in fig. 1. In some cases, the visible arms are fixed and the pattern seems to be star-like ((d), (g) and (h) in fig. 1). All the observed patterns are robust. Even though a strong external perturbation can break a pattern, the system restores it rapidly. Further increase of Q leads to bubble emergence at the liquid surface with two different intervals. Bubbles emerge alternately at one of these two time intervals after the preceding one. This is a consequence of an instability in bubble chains [17], leading to bubble pairing and period doubling behavior. Patterns formed by paired bubbles are beyond the scope of the present paper and will not be considered hereafter.

The divergence angles measured for different oils are presented in fig. 5(a) and (b). Their behavior with increasing Ω is shown in fig. 5(a). A bifurcation from the alternate ($\psi = \pi$) to spiral ($\psi = \pi$) modes is found at different critical values of $\Omega = \Omega_{\mathrm{cr}}$ for different oils. This bifurcation is discussed in detail in sect. 4.1. In fig. 5(b), the results of the same measurements are plotted in the Ω-Oh plane, where the divergence angles are shown by iso-value curves. Groups of experimental points around a constant value of Oh are obtained by experiments with the same oil. On this diagram, one can see parameter values yielding spiral patterns on the surface. The shaded regions in the diagram correspond to the region where patterns in the alternate mode were observed and the region of bubble emergence with two intervals. As discussed in sect. 3.2, the divergence angle ψ depends also on the Bond number Bo. The Bo dependence can be found from the present diagram by noting that the product $BoOh^4 (= g\mu^2/\rho\gamma^3)$ acquires a constant value for a given liquid. This product is identical to the Haberman-Morton number and takes a value of 0.0016, 0.0061, 0.031 and 0.097 for the oil of 0.033, 0.048, 0.072 and 0.097 Pa s, respectively.
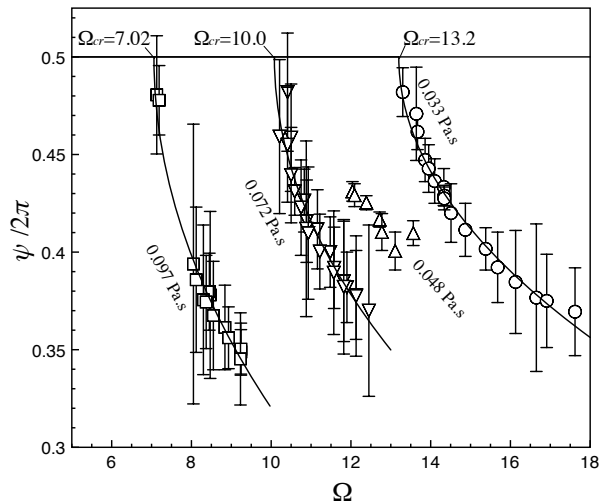
(a) Normalized divergence angles showing a bifurcation from an alternate pattern ($\psi = \pi$)
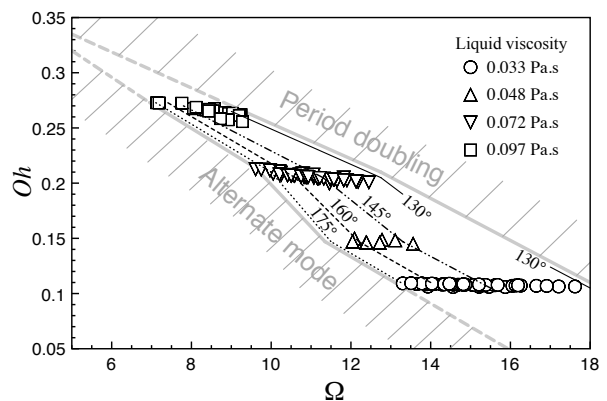
(b) Divergence angles in degree shown by iso-value curves on the Ω-Oh plane

Fig. 5. Divergence angle dependence on the control parameters. In (a), curves in bold lines are the least-square fits in the form of eq. (2). The error bars represent standard deviations from the averaged values. Experimental parameters (d, H) in mm are: $(0.8, 87)$ for the oil of $0.033\,\mathrm{Pa\,s}$; $(0.8, 94)$ and $(1.2, 119)$ for $0.048\,\mathrm{Pa\,s}$; $(1.4, 78)$ and $(1.4, 86)$ for $0.072\,\mathrm{Pa\,s}$; $(1.2, 78)$ for $0.097\,\mathrm{Pa\,s}$.

It is seen that, as the frequency increases for a given liquid, the divergence angle decreases until the onset of period doubling at a certain Ω. For a larger value of Oh, this critical value of Ω becomes smaller and the range of Ω for spiral patterns becomes smaller. This may suggest that with a sufficiently large viscosity (*i.e.*, a large Oh) no spiral pattern might be observed. Indeed, in preliminary experiments, we did not succeed in forming any patterns with an oil of $0.17\,\mathrm{Pa\,s}$. On the other hand, in an oil of small viscosity, the rising path of released bubbles was destabilized and zigzag or helical paths were observed [18]. The emerged bubbles did not form any regular patterns any more. Hence, the pattern formation concerns a limited region of the parameter plane.

4 Discussion

4.1 Bifurcation from the alternate mode

The generation of different patterns is related to different values of the divergence angle ψ. In particular, its departure from the constant value π reflects bifurcation from the alternate to spiral modes accompanied by breaking symmetry. As seen in fig. 5(a), below a critical value Ω_{cr}, the divergence angle is equal to π, corresponding to the alternate mode. Above Ω_{cr}, the order parameter ψ decreases. In the experiments, no hysteresis was observed in proximity of the bifurcation point, within the accuracy of the measurements. The experimental data group well around the expected fits for a supercritical bifurcation, as shown by the bold line curves in the figure. For experiments with the oil of 0.048 Pa s, no fit was determined because the experimental conditions are farther away from the bifurcation point. The fits shown in the figure are

$$\frac{\psi}{2\pi} = 0.5 - \alpha \left(\frac{\Omega}{\Omega_{\mathrm{cr}}} - 1 \right)^{0.5}, \qquad (2)$$

where α and Ω_{cr} are fitting parameters. Their values are $(\alpha, \Omega_{\mathrm{cr}}) = (0.236, 13.2), (0.273, 10.0)$ and $(0.275, 7.02)$ for the experiments with the oil of 0.033, 0.072 and 0.097 Pa s, respectively. The parameters α and Ω_{cr}, respectively increase and decrease as the liquid viscosity increases. The dependence of the parameters α and Ω_{cr} on the dimensionless groups Oh and Bo will be examined in a future publication.

4.2 Relation with phyllotaxis

For a given surface image with bubbles moving radially, the divergence angle ψ is determined unambiguously. Nevertheless, there is no intuitive relation between a value of ψ and a pattern, as noted by Bravais [3,4]. The observer's eyes are attracted at first sight by a number of rotating or fixed arms formed by bubbles and recognize a pattern. These arms are what Bravais called *conspicuous* and are only apparent features of the patterns.

As noted by Shimper [3], a divergence angle can often be related to an irreducible rational fraction as $\psi = \frac{n}{m} \cdot 2\pi$. The denominator m corresponds to the number of fixed arms and equals the number of successive bubbles necessary to recover the same emission direction: the $(m+1)$-th bubble is emitted in the same direction as the first emitted bubble. The numerator n is what Bravais called the *encyclic number* and is associated with the total angular rotation during the emission of m successive bubbles: $\theta_{j+m} - \theta_j = 2\pi n$ (see fig. 3). Figure 1(d), showing a pattern of seven fixed arms, for example, is formed with a divergence angle of $0.4275 \cdot 2\pi$ rad ($= 153.9°$). This angle can be associated with a rational fraction $\frac{3}{7}$ ($= 0.4286$). A pattern of rotating arms can also be associated to a rational divergence angle. Recognition of rotating arms instead of fixed arms comes from the fact that the deduced m

is too large with respect to the number of bubbles moving simultaneously on the surface. They are not numerous enough to reveal the hidden fixed star. In fig. 1(b), the measured ψ value equals $0.46167 \cdot 2\pi$ rad ($= 166.2°$) and the nearest relevant fraction is $\frac{6}{13}$ ($= 0.46154$). This implies that thirteen fixed arms will be exhibited by the emission with this divergence angle, if enough bubbles coexist on the surface. However, the observer links spontaneously emitted bubbles in each double period $2T$ and considers the pattern as one of the rational fraction $\frac{1}{2}$ in rotation. This recognition of the pattern is associated with the fact that in the continuous fraction writing of the divergence angle, the rational approximation preceding $\frac{6}{13}$ is $\frac{1}{2}$: $0.46167 = 1/(2 + 1/(6 + 1/\cdots))$. The error coming from the worse approximation by $\frac{1}{2}$ is what makes the two arms rotate.

These observations demonstrate experimentally Bravais's mathematical point: the observed pattern depends on two parameters, not only on the divergence angle ψ (as Shimper assumed), but also on the radial distance Δr between two successive elements. If they are far apart from each other, the pattern corresponding to the relevant rational fraction is not observed. Instead, the pattern of the previous approximation in the continuous fraction is recognized. For the pattern generated by a given divergence angle ψ, one can see a successive number of arms by changing the radial distance of the elements. These patterns correspond to the successive rational approximations in the continuous fraction for ψ. Bravais also showed that all the elements of the Fibonacci sequence $\{1, 1, 2, 3, 5, 8, 13 \ldots\}$ are observed by varying the radial distance if, and only if, the divergence corresponds to the golden mean $\psi = \psi_G \approx 0.764\pi$. In the present experiments, the divergence ψ varies continuously from π to 0.72π with varying Q and does not remain around ψ_G. Consequently, patterns with the number of arms m not included in the Fibonacci sequence are observed, *e.g.*, such as the seven and nine arms shown in fig. 1(c), (d) and (e).

To understand the continuous variation of ψ and its relation to patterns, one has to come back to the work of van Iterson and followers [3,7,15,19,20]. For patterns constituted by elements with a finite size (like bubbles in the present study) and not by mathematical points (like in Bravais's work), the packing and contacts between the elements are important in pattern determination. Elements in contact constitute parastichies, which are characterized by the numbers of right and left parastichies m_1 and m_2. For a given pair (m_1, m_2), van Iterson computed geometrically possible values of the divergence and the separation. The latter values are, for example, related by the following equation for elements packed on the surface of a cylinder (see eq. (4a) in [15]):

$$(m_1^2 - m_2^2)\Pi^2 = \left(m_2 \frac{\psi}{2\pi} - p \right)^2 - \left(m_1 \frac{\psi}{2\pi} - q \right)^2, \quad (3)$$

where Π is the normalized separation defined by $\Pi = \Delta r/C$ (C is the size of the packing domain, *i.e.*, the circumference of the cylinder). This parameter reflects the importance of packing: the smaller Π is, the more packed
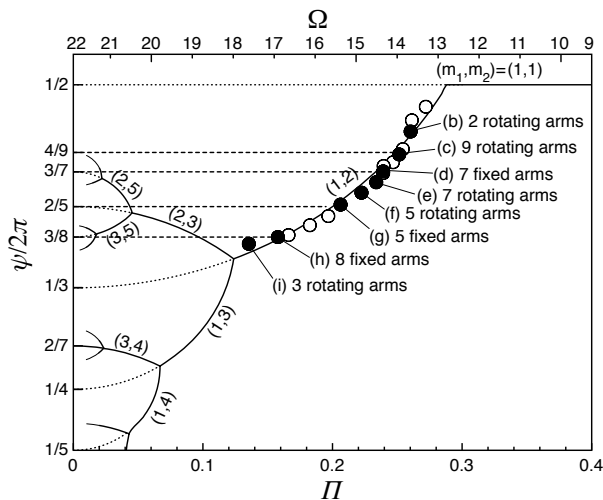
Fig. 6. van Iterson diagram with experimental data obtained with the silicone oil of 0.033 Pa s. Full circles are the data of the experiments shown in fig. 1.

the elements are. The other parameters in (3), q and p, are the closest integers to $m_1\psi/2\pi$ and $m_2\psi/2\pi$, respectively. These are the encyclic numbers introduced by Bravais. Equation (3) gives a tree of successive bifurcations in the divergence-separation plane, each branch being characterized by a pair of parastichy numbers (m_1, m_2). This van Iterson diagram is shown in fig. 6. In the figure, some of the simple rational fractions $\frac{n}{m}$ are shown on the ordinate axis. If the divergence angle is around one of these values, the number of arms recognized in a small physical system is expected to equal its denominator m. In the diagram, as Π decreases, a symmetry breaking bifurcation corresponding to the transition from the opposite deposition $(m_1, m_2) = (1, 1)$ to the spiral pattern $(1, 2)$ is first observed. The divergence ψ decreases on the branch $(1, 2)$ until the point $\Pi \approx 0.12$ where the second bifurcation occurs. One of the two branches $(1, 3)$ and $(2, 3)$ follows when Π decreases further. Another bifurcation occurs at the end of each branch.

In the present experiments, the control parameter affecting the packing is the bubble formation frequency Ω. As the frequency increases, the number of bubbles interacting in the deformed surface zone increases from two to three, as seen in *e.g.*, fig. 4. Hence, if the present pattern formation has a phyllotactic character, the experimental data will follow the van Iterson diagram with a decreasing Π when Ω increases. In fig. 6, the experimental points reported in fig. 5(a) for the oil of 0.033 Pa s are plotted after transforming the frequency Ω to the separation Π through the relation $\Pi = 0.692 - 0.0316\Omega$. This linear transformation was determined by the least-square procedure so that the experimental data group the best around branches of the van Iterson diagram. It is seen that all the points are on the branch $(1, 2)$ and the observed first symmetry breaking bifurcation corresponds to the transition from branch $(1, 1)$ to branch $(1, 2)$. As mentioned earlier, the patterns with $\psi = \pi$ coincide with the inter-

action between two bubbles at the surface (see fig. 4(a)). Those with $\psi < \pi$ are observed when three bubbles interact with each other (see fig. 4(b)). In the iterated process considered by Douady and Couder, an increase in the number of effectively interacting elements (ferrofluid drops) is also noticed at the bifurcation from the alternate mode [11,12]. This similarity further suggests that bubbles create real phyllotactic patterns of self-packing elements and not "spiral printings" which are yielded by successive depositions of elements with a divergence angle fixed from outside (like the spiraling of a fluid [16]). The observed bifurcation in the present experiments shows that the divergence is fixed through the interactions between emerging bubbles.

5 Conclusion

Patterns formed by centimeter scale bubbles emerging periodically at a liquid surface were examined with the intention of studying the analogy to phyllotaxis. Different conspicuous patterns were observed in these experiments. Measurement of the divergence angle ψ revealed the first symmetry breaking bifurcation corresponding to the alternate-spiral transition of the van Iterson diagram. This suggests that the observed patterns are formed through the packing mechanisms of the elements (bubbles), which is similar to phyllotaxis. Further characterization of the system by measuring the bubble-induced advection flows and observing in detail the packing of bubbles at the emergence point is being performed and will be reported in future publications.

References

1. Theophrastus, *Inquiry into plants* (G. P. Putnam's Sons, translation by Sir Arthur Holt, London, W. Heinemann, New York, 1916).
2. J.P. Richter, *The Notebooks of Leonardo da Vinci* (Dover Publications, New York, 1970).
3. I. Adler, D. Barabé, R. Jean, Ann. Botany **80**, 231 (1997).
4. L. Bravais, A. Bravais, Ann. Sci. Nat. second series **7**, 42 (1837).
5. L. Bravais, A. Bravais, Ann. Sci. Nat. second series **8**, 11 (1937).
6. W. Hofmeister, Handb. Physiol. Botanik **1**(2), (1868).
7. G. van Iterson, *Mathematische und Mikroskopisch-Anatomische Studien über Blattstellungen nebst Betraschtungen über den Schalenbau der Miliolinen* (GustavFischer Jena, 1907).
8. C. Kuhlemeier, Trends Plant Sci. **12**, 1360 (2007).
9. L.S. Levitov, Phys. Rev. Lett. **66**, 224 (1991).
10. C. Nisoli, N.M. Gabor, P.E. Lammert, J.D. Maynard, V.H. Crespi, Phys. Rev. E **81**, 046107 (2010).

11. S. Douady, Y. Couder, Phys. Rev. Lett. **68**, 2098 (1992).
12. S. Douady, Y. Couder, J. Theor. Biol. **178**, 255 (1996).
13. S. Douady, Y. Couder, J. Theor. Biol. **178**, 275 (1996).
14. S. Douady, Y. Couder, J. Theor. Biol. **178**, 295 (1996).
15. S. Douady, in *Symmetry in Plants*, edited by R.V. Jean, D. Barabé (World Scientific, Singapore, 1998), chapt. 14 "The selection of phyllotactic patterns", pp. 335–358.
16. M. Habibi, P. Moller, N. Ribe, D. Bonn, EPL **81**, 38004 (2008).
17. M.C. Ruzicka, Int. J. Multiphase Flow **31**, 1063 (2005).
18. A. Prosperetti, Phys. Fluids **16**, 1852 (2004), Section V, "Leonardo's paradox".
19. R.O. Erickson, Science **181**, 705 (1973).
20. P. Atela, C. Golé, S. Hotton, J. Nonlinear Sci. **12**, 641 (2002).